Maryam Zarghami Dehaghani, Thomas Fabiani and
Maria Grazia De Angelis*

5 Chemical engineering contribution to hemodialysis innovation: achieving the wearable artificial kidneys with nanomaterial-based dialysate regeneration

Abstract: Hemodialysis (HD) has long been a cornerstone in the renal replacement therapy for end-stage kidney disease (ESKD), primarily through conventional in-center HD. Current HD systems in hospitals are bulky, water-demanding, and constrain the mobility and quality of life of ESKD patients. Home HD (HHD) offers the chance of delivering more frequent treatments close to the patient, reducing vascular stress and post-treatment hangover and improving patients' lifestyles. However, current HHD devices are analogous to hospital machines, requiring significant space, costly renovations, and they are energy and water intensive. Miniaturisation of HD systems depends on the reduction of water consumption, requiring the introduction of a dialysate regeneration unit, that purifies the spent dialysate of uremic toxins (UTs) and recirculates it, cutting down the amount of dialysate needed. This represents a crucial step for the development of a wearable artificial kidney. However, regenerating dialysate poses significant technical challenges as it involves separating a complex mixture under strict biomedical safety and stability requirements. This paper provides an engineering perspective into current research on using nanomaterials for adsorbing UTs from spent dialysate.

Keywords: hemodialysis; wearable artificial kidney; uremic toxins; nanomaterials; adsorption

5.1 Introduction

5.1.1 Kidney functionality and uremic toxins

Kidney functionality is classified into four primary categories:

***Corresponding author: Maria Grazia De Angelis**, School of Engineering, Institute for Materials and Processes, University of Edinburgh, King's Buildings, Robert Stevenson Road, EH9 3FB, Edinburgh, SCO, UK, E-mail: grazia.deangelis@ed.ac.uk. https://orcid.org/0000-0002-1435-4251
Maryam Zarghami Dehaghani and Thomas Fabiani, School of Engineering, Institute for Materials and Processes, University of Edinburgh, King's Buildings, Robert Stevenson Road, EH9 3FB, Edinburgh, SCO, UK, E-mail: mzargham@ed.ac.uk (M. Zarghami Dehaghani), T.Fabiani@sms.ed.ac.uk (T. Fabiani)

As per De Gruyter's policy this article has previously been published in the journal Physical Sciences Reviews. Please cite as: M. Zarghami Dehaghani, T. Fabiani and M. G. De Angelis "Chemical engineering contribution to hemodialysis innovation: achieving the wearable artificial kidneys with nanomaterial-based dialysate regeneration" *Physical Sciences Reviews* [Online] 2024. DOI: 10.1515/psr-2024-0055 | https://doi.org/10.1515/9783111394558-005

- excretory, namely the elimination of waste products of protein metabolism (such as urea, creatinine, and ammonia), drugs and their metabolites.
- regulatory, involving the control of body fluid volume and its composition, maintaining electrolyte balance and acid-based balance.
- endocrine, related to the production of hormones including erythropoietin, renin and prostaglandins to regulate various physiological processes.
- metabolic: the kidney converts inactive vitamin D (second hydroxylation of vitamin D, calcidiol) into its active form (calcitriol or 1,25 di-hydroxycholecalciferol) which is essential for calcium homeostasis [1].

A kidney receives one-quarter of the blood cardiac output every minute and approximately consists of one million of functional units, named nephrons. Each nephron operates as an independent entity, consisting of the glomerulus (the actual filtration unit) and the renal tubule. Blood flows from the heart to the kidneys through the renal arteries, and is filtered in the glomerulus, where an ultrafiltration process is propelled by hydrostatic pressure gradient of approximately 10 mmHg (1.33 kPa) so that small molecules, water, and ions pass through the filtration barrier and enter the Bowman's capsule, while larger molecules like blood proteins and cells are retained [2]. The permeate flows through the renal tubule, where water, electrolytes, glucose, and amino acids are reabsorbed into the bloodstream, while waste products are secreted to form urine [3].

Factors such as diabetes mellitus, hypertension, inflammation of the glomeruli (glomerulonephritis), urinary reflux and infections (pyelonephritis), and polycystic kidney disease can cause the gradual loss of functioning nephrons over time, leading to lower filtration activity. As a result, solutes accumulate and they are designated as uremic toxins (UTs) when they disrupt normal biological functions causing the so-called uremic syndrome [4, 5], which is of growing interest in the biological and clinical research. There are three main categories of UTs associated with chronic kidney disease (CKD) [4, 6] as reported below:

1) Small, free water-soluble UTs (<500 Da) such as uric acid, urea, creatinine, oxalate, guanidine, hyaluronic acid.
2) Small molecular weight (<500 Da), protein-bound UTs (PBUTs): these UTs may bind on proteins present in blood, therefore the low UTs concentration in blood makes the clearance challenging. Examples include indoxyl sulfate, and p-cresyl sulfate (*p*-CS).
3) Middle and large-size (>500 Da) such as cystatin C, leptin, β2-microglobulin.

UTs can be classified based on other parameters such as chemical similarities, metabolic pathway, or toxicity as summarised in the minireview by Myjak et al. [4]. In the review paper by Vandholder et al. [7] it is reported that the most toxic UTs, in descending order, include: p-cresyl sulfate, beta-2 microglobulin, asymmetric dimethylarginine (ADMA), kynurenines, carbamylated compounds, fibroblast growth factor-23 (FGF-23), interleukin-6 (IL-6), tumor necrosis factor-α (TNF-α), and symmetric dimethylarginine (SDMA).

5.1.2 Chronic kidney disease and hemodialysis design

Chronic kidney disease is defined as the decline of the glomerular filtration rate (GFR) to less than 60 mL/min per 1.73 m^2 of body surface, or by detection of albuminuria, haematuria (>30 mg g^{-1}), or abnormalities in urine sediment for at least three months [1]. Annually, CKD is responsible for approximately 1.2 million fatalities globally, underscoring its significant impact on individual health and healthcare systems [8]. CKD is classified into five phases, with the most severe stage referred to as end-stage kidney disease (ESKD) associated with GFR less than 15 mL/min per 1.73 m^2, which requires a renal replacement therapy (RRT), such as hemodialysis (HD) or transplantation [9, 10]. According to the European Renal Registry [11], only 4 % of the patients in RRT had the chance to receive a transplant due to the scarcity of kidneys. According to the Global Kidney Health Atlas published in 2019, approximately 14.5 million people around the world will have developed ESKD by 2030 [12]. Therefore, developing and updating HD systems still remains a topic of research so that individuals with ESKD can maintain a more stable health status, alleviate symptoms, and prolong survival.

5.2 Basic equipment of conventional hemodialysis

HD involves the exchange of UTs, ions and excess fluids between the blood stream and a fluid, called dialysate, through a semipermeable membrane embedded in a housing unit, named dialyser [13]. Figure 5.1a and b demonstrate the equipment of the HD machine and configuration of the dialyser, respectively. Figure 5.1a shows that the patient's blood is drawn from a vascular access and passes through a series of controls, including an arterial pressure meter and a heparin pump to prevent clotting. The blood pump then propels the blood with a rate between 200 and 500 mL/min through the dialyser. In the dialyzer, UTs and excess fluids pass from the blood into the dialysate solution [14]. The dialyser is a module formed by a bundle of hollow fiber membranes designed to mimic glomerular filtration, namely retaining serum proteins, e.g., human serum albumin [15], and blood cells, but able to maximize the clearance of UTs ranging from a few tens of Daltons to 11 kDa. The dialyzer consists of approximately 10,000 to 20,000 thin fibers running longitudinally through the device (as shown in Figure 5.1b), each with an inner dimension ranging from 150 to 250 μm, and thickness between 7 μm and 50 μm and a length of 150 mm. It employs a countercurrent flow mechanism, where blood flows inside the fibres and dialysate flows on the outside [14, 16]. Considering the pore size determining the hydraulic permeability (volume passing through the membrane per unit surface area, time, and pressure), dialysers are classified into **low-flux** (pore radius between 2 and 3 nm, permeability in the range of 10–20 mL m^{-2} h^{-1} $mmHg^{-1}$) and **high-flux** (pore radius between 3.5 and 5.5 nm and permeability in the range of 200–400 mL m^{-2} h^{-1} $mmHg^{-1}$) membrane [17].

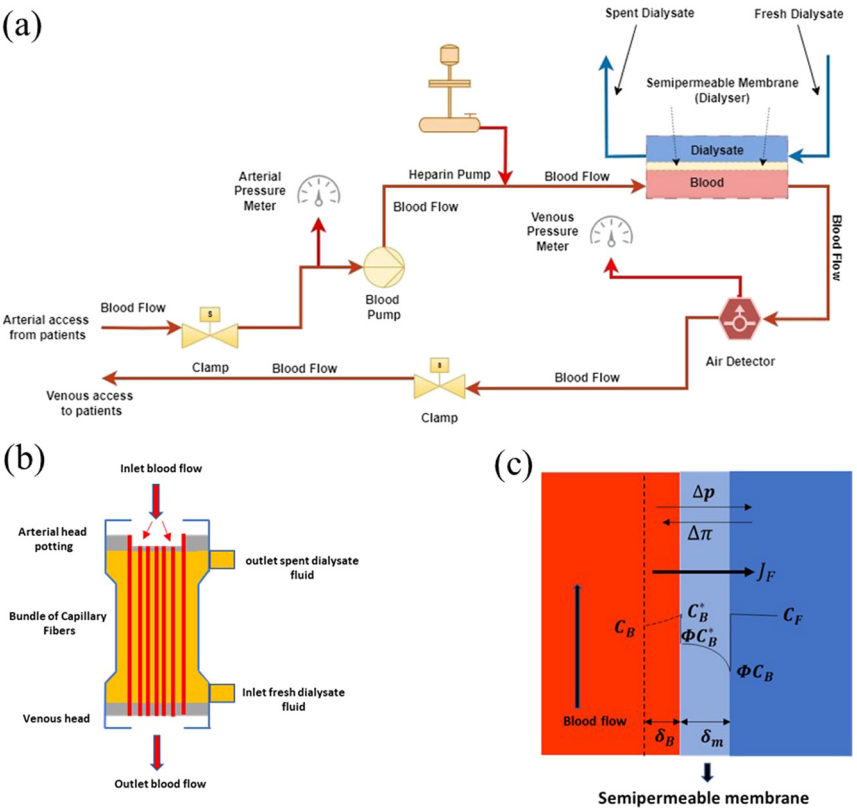

Figure 5.1: Conventional HD equipments. (a) The diagram of conventional HD, (b) the schematic of dialyser having hollow fibres, (c) convective solute transport across a semipermeable membrane in a hemodiafiltration process. Symbols are defined in the text.

Dialysate flows in the whole system with the rate of 600–800 mL min^{-1}. Dialysate is the solution that interacts across a membrane with a patient's blood during dialysis, carrying away waste products and excess fluids from blood without mixing with it. It plays a dual role: removing UTs while adding essential ions, such as calcium and bicarbonate, to maintain pH balance and electrolyte levels. Tailored to match the patient's required solute concentrations, dialysate prevents unwanted fluid shifts by closely matching blood osmolality, and specific concentration gradients drive the diffusion of solutes across the membrane. Key components, such as sodium and bicarbonate, may enter the blood, balancing the patient's electrolyte levels. Modern HD systems precisely regulate the dialysate's composition, temperature, and flow rate to optimise treatment and control fluid removal. Table 5.1 shows the composition of commercial dialysate.

The major components of the conventional dialysate circuit, shown in Figure 5.2, include: 1) water treatment section, 2) heating and deaeration component to warm the

Table 5.1: Dialysate commercial composition [18].

Compound	Concentration in dialysate
Sodium (Na^+)	134–145 mM
Potassium (K^+)	0–4 mM
Calcium (Ca^{2+})	1.25–1.75 mM
Magnesium (Mg^{2+})	0.5–0.75 mM
Acetate/Citrate	2–4
Chloride (Cl^-)	98–124 mM
Bicarbonate (HCO_3^-)	30–40 mM
Dextrose	11
Glucose	0–2 gL^{-1}
PH	7.1–7.3
P_{CO2}(mmHg)	400–110

dialysate to body temperature and removing bubbles, 3) proportioning section to mix the concentrate solutions (acid and bicarbonate) with ultrapure water to create the fresh dialysate with the correct chemical composition to maintain the proper electrolyte balance, 4) monitoring system to check the composition, temperature, and flow rate of the dialysate, 5) volumetric control component to adjust the transmembrane pressure to ensure that the appropriate amount of fluid is extracted as ultrafiltrate (UF), the fluid permeated through the membrane during the dialysis session [19]. Every session approximately demands 120 L of the dialysate [20, 21].

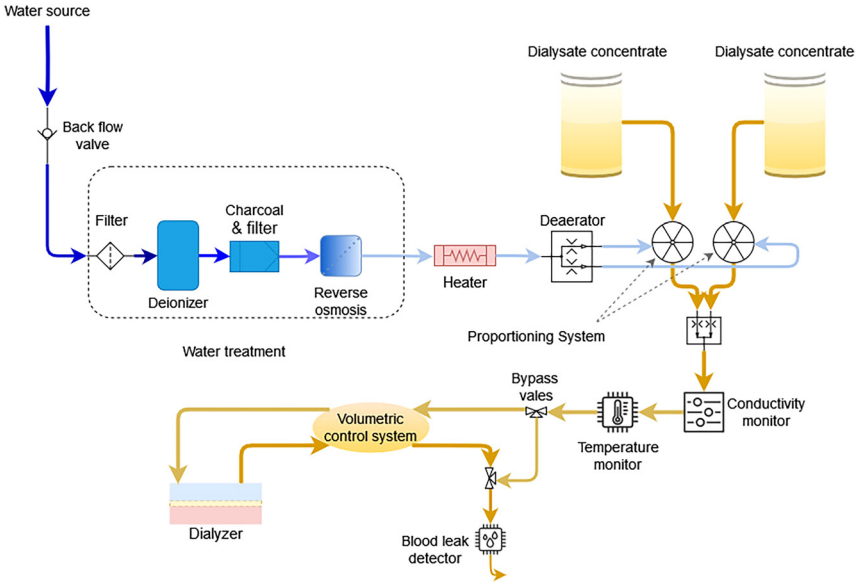

Figure 5.2: Conventional dialysate circuit.

Dialyser **clearance**, a parameter to evaluate the performance of dialyser, is defined as the amount of blood cleared in a minute $\left(K = \frac{Q_{B,in}C_{B,in} - Q_{B,out}C_{B,out}}{C_{B,in}}\right)$ where Q_B refers to the blood flow rate at the inlet $Q_{B,in}$ and outlet $Q_{B,out}$ of the dialyser and C_B gives the corresponding concentration [22]. Urea concentration decreases over time during the session using the principle of exponential decay. The dimensionless parameter Kt/V, derived from a single-compartment kinetic model ($C_t = C_0 e^{Kt/V}$), is used as an index of HD adequacy or dosing. K is the urea dialyser clearance, t is the time of the session, and V refers to the distribution volume [23].

The movement of UTs across a semipermeable membrane is controlled by the physiochemical properties of the molecule, the permeability of the membrane and the operational conditions such as blood flow and dialysate flow rates [14].

Notably, increasing flow rates mainly enhances the clearance of small UTs by minimising boundary layer effects, but it has little impact on larger solutes (e.g., myoglobin, molecular mass 17 kDa), where the membrane is the primary resistance to mass transfer [16].

Standard membrane dialysers with small pores, known as low-flux membranes, rely mainly on diffusion-based mass transfer and are limited in their ability to remove middle molecules due to their restricted pore size. To address this issue, **high-flux** dialysers are used, which have higher **membrane pore size** that facilitate the removal of the larger "middle" molecules such as the beta-2 microglobulin which leads to the dialysis-related amyloidosis.

In **hemodiafiltration**, a novel therapeutic strategy, concentration gradient-driven diffusion is augmented by **convection**, as depicted in Figure 5.1c, that is driven by a net pressure gradient (Δp-$\Delta\pi$) where Δp and $\Delta\pi$ correspond to **hydrostatic** and **osmotic** pressure difference across the membrane, respectively. The flow associated to this mechanism (J_F), called ultrafiltration rate, is equal to the net pressure difference multiplied by the **hydraulic permeability** L_p of the semipermeable membrane, that is related to the membrane thickness, pore geometry and fluid properties [24].

Osmotic pressure $\Delta\pi$ depends on the concentration of impermeable solutes in blood and dialysate. At a section of dialyser close to the blood inlet, due to the high concentration of solutes in the blood, the osmotic pressure difference may balance the hydrostatic pressure difference, leading to a reversal of the pressure gradient across the membrane, resulting in flow from dialysate to blood (**back filtration**) [16]. This may cause re-entry of contaminants from the dialysate into the bloodstream [25–27].

According to **stagnant film theory**, the blood concentration of larger solutes close to the membrane interface, in the so-called "**boundary layer**" δ_B becomes larger than in the bulk, reaching a maximum close to the membrane interface ($C_B^* > C_B$). The phenomenon is called **concentration-polarisation** and is exacerbated at high ultrafiltration rates. The equilibrium **partition coefficient** (Φ) describes how substances distribute between the membrane and surrounding fluids.

A **sieving coefficient** $SC = C_F/C_B$, representing the ratio of solute concentration in the filtrate, C_F, versus the same molecule concentration in the blood, C_B, measures the fraction of solute passing through the membrane, and depends on the relative size between the molecule and the pore. Solutes like urea and creatinine, which are much smaller than the membrane pores, have *SC* values near 1, indicating efficient permeation. Larger solutes with sizes exceeding pore dimensions have *SC* values close to zero. For solutes near the membrane's molecular mass cut-off, *SC* values are typically below 0.1. Manufacturers aim for *SC* values above 0.6 for β2-microglobulin and below 0.008 for albumin (66.5 kDa) [28]. As depicted in Figure 5.1c, *SC* is affected by concentration polarisation: indeed, the actual sieving coefficient ($SC_a = C_F/C_B^*$) which accounts for middle-size solute accumulation near the membrane ($C_B^* > C_B$) becomes lower than the nominal value especially at high ultrafiltration rates, reducing the membrane's selective filtering and increase useful protein (e.g. albumin) loss. Careful management of ultrafiltration rates through tuning the membrane pore size, alongside blood flow rates, is crucial in balancing toxin clearance and preventing albumin loss in HDF [16].

5.3 Developing dialysate regeneration techniques for the wearable artificial kidney

Conventional HD is generally delivered in three sessions per week, requiring the patient to be in hospital for three or 4 h per session. Moreover, commercial HD machines limit patients' mobility and daily activities, having a detrimental impact on the quality of life [29]. Exploring alternatives to this traditional schedule could potentially enhance patient survival, reduce treatment burden, and elevate overall well-being. Extended or more frequent dialysis sessions have been shown to lessen cardiac stress, regulate blood pressure, and boost metabolic health, underscoring the potential benefits of portable HD devices in improving patient lifestyle [30].

The process of regenerating spent dialysate is critical for the development of portable or wearable HD devices, as it enables the reduction of water use and the downsizing of equipment, eliminating the need for a direct water supply. The primary task of a regeneration unit is to keep uremic toxin concentrations low in the dialysate to ensure effective dialysis. While small, water-soluble uremic toxins like urea are readily removed during HD, making them the most concentrated solutes in the dialysate, certain UTs prove challenging to eliminate. Factors such as larger molecular size or strong protein binding can hinder their removal; these toxins typically appear in lower concentrations in the dialysate and are more difficult to clear efficiently. Amino acids including proline, valine, glycine, glutamate, alanine, leucine and other non-toxic compounds, such as glucose, L-lactate, and glycerol, are also present and can affect the separation process. The details on the amount of each solute removed during HD and their presence in spent dialysate

are reported in a review paper by Shao et al. [31]. Efficient dialysate regeneration requires addressing these complexities to ensure effective UTs removal while maintaining essential physiological compounds.

5.3.1 Regeneration of spent dialysate: technologies for uremic toxins elimination

Urea, uric acid, and creatinine are small, water-soluble toxins are easily removed during HD and, as a result, are present in higher concentrations in the spent dialysate. Therefore, most researches focused on optimizing the removal of these molecules from spent dialysate. It must be noticed, however, that other toxins, e.g. protein-bound uremic toxins, present in smaller quantities in blood, are hard to eliminate with standard dialysers due to their larger size but they may be even more toxic. Such substances are believed to cause the uremic syndrome which is observed only in HD patients and not in transplanted ones, due to the incomplete removal of UTs of the HD membrane compared to a working kidney, and are associated to worse health status and higher mortality of HD patients. This requires for an interdisciplinary effort where chemical engineers work in close cooperation with nephrologists and biologists to identify and remove all harmful substances from the blood of the patients and, consequently, from the regenerated dialysis fluid.

Enzymatic conversion of urea. Urease has been used to oxidize urea into ammonium and carbon dioxide with high selectivity. The first portable HD device, the recirculating dialysis (REDY) sorbent system marketed from 1973 to 1993, performed dialysate regeneration through a multi-cartridge technology and weighed 5 kg (including dialysate) [20]. In the REDY system, in the first layer, non-urea organic compounds such as heavy metals, oxidants, chloramines, and other organic molecules were adsorbed by activated carbon. In the second layer, urea was enzymatically converted to ammonium and carbonate ions by immobilized urease. Ammonium was then captured by a cation exchanger of zirconium phosphate, which also removed calcium, magnesium, potassium, and other metal cations, releasing sodium and hydrogen. In the final layer, anions like phosphates and fluoride were absorbed by zirconium oxide and zirconium carbonate, through exchanging bicarbonate and acetate. The issue of leachate of aluminium used to immobilize urease, that was deemed responsible for severe side effects, led to its removal from the market. A similar device based on sorbent layers and immobilized urease named WAK (Wearable Artificial Kidney) was fabricated by Gura et al. [32]: this device underwent clinical trials but encountered issues with CO_2 bubble formation, due to the chemical decomposition of urea by urease, and flow control. Other prototypes similar to the REDY devices have been summarized in the review paper by Gelder et al. [20].

Integration of HD with FO. Another technique proposed to purify part of the dialysate and reduce the water demand of HD is forward osmosis (FO). Although strictly not employed to produce wearable dialysis devices, such technique can be used to regenerate dialysate and is thus included in the present review. Figure 5.3 shows the

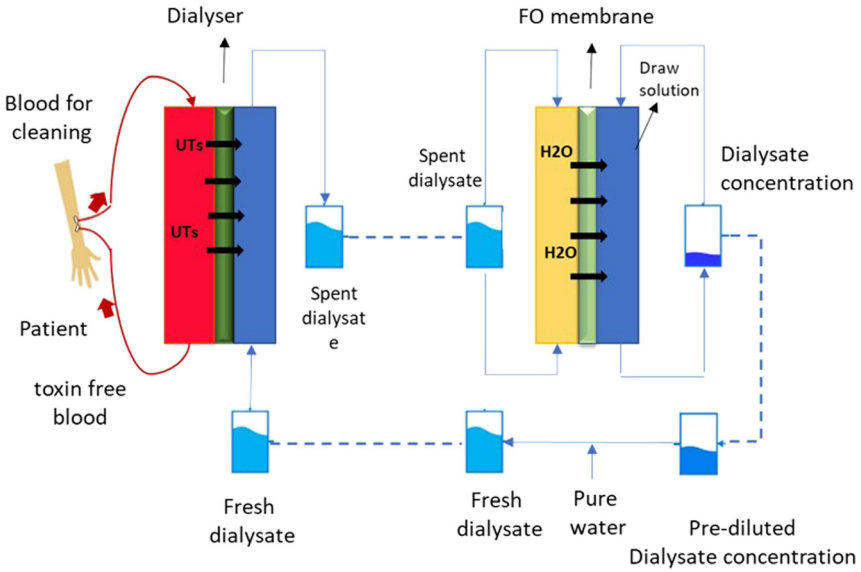

Figure 5.3: Diagram of the integration of HD with spent dialysate recovery through FO process.

schematic of the integration of HD with spent dialysate recovery through FO process. In such a process, water permeates through a semipermeable membrane to reach a draw solution, at higher osmolarity.

Commercially available dialysate concentrates can be used as a draw solution to recover clean water from the spent dialysate. Initial urea concentrations in spent dialysate and blood are 5 mM and 23 mM, respectively. The performance of FO process for regeneration of spent dialysate has two limiting cases: ideal conditions with complete urea rejection, or complete water recovery and minimal urea rejection, which is undesirable since it indicates that almost all urea remains in the dialysate [33]. FO membranes demonstrate a high rejection rate for compounds found in significant concentrations in the dialysate, including ions, glucose, and charged molecules. However, the rejection rate for urea remains comparatively low and is heavily affected by its concentration [34].

Photo-electrocatalytic oxidation. Such a technique leverages light and catalytic materials to facilitate chemical reactions, specifically for oxidizing urea into molecular nitrogen and carbon dioxide. This approach offers the advantages of low power consumption by using LED technology and disadvantages of by-products and low selectivity of oxidation [35, 36].

Adsorbents. One of the most studied strategies uses adsorbents to capture UTs from the dialysate. Porous materials, characterized by their elevated specific surface area, represent an excellent option as sorbents, due to their ability to maximize adsorption capacity, by presenting a high number of adsorption sites to the liquid phase. The dimensions and configurations of the pores, as well as the surface functionalization, play

significant roles in influencing adsorption phenomena within the material, providing diverse binding sites for adsorbates [37]. UTs accumulates onto the solid surface of the adsorbent through dispersion forces, hydrogen bonding, electrostatic interactions, polarization, and covalent bonding [38]. The efficacy of the process is given by the static binding capacity, defined as the amount of adsorbate adsorbed per unit mass of adsorbent in equilibrium with a certain concentration of the solute in the liquid. Adsorbents used for UTs adsorption include nanoporous materials and dense polymers (chitosan, starch, and cellulose), as well as mixed matrix membranes composed of a polymer matrix embedding adsorbent particles [39]. The review paper by Gelder et al. [40] provides a summary of urea removal strategies for the regeneration of spent dialysate. Urea is the most abundant toxin in spent dialysate, and the harder to abate with conventional adsorbents: therefore, traditional adsorbent materials have too low binding capacity towards urea to be used in a wearable dialysis device. However, thanks to the advances in nanotechnology, new materials to be employed as adsorbed have been synthesized, such as metal organic frameworks and covalent organic frameworks, with great structural tunability, that could potentially be designed to remove hard-to-abate molecules like urea. A classification of different adsorbent nanoporous materials and their binding capacity towards urea at the typical average concentration in the dialysate is reported in the following section.

5.3.2 Adsorption materials for UT removal

Activated carbon (AC) is widely studied for its UTs adsorption capacity, but achieving the adsorption of the daily production of urea requires a large quantity of material [36, 41]. As a result, research has shifted towards exploring materials with controlled and/or ordered porosity such as zeolites, mesoporous silica, metal-organic frameworks (MOFs), MXenes, and molybdenum disulfide (MoS_2), which have shown potential for enhanced physisorption of UTs. Additionally, these sorbents can be incorporated into mixed matrix membranes (MMM), where they effectively adsorb UTs while allowing water to pass through the membrane [42].

5.3.2.1 Experimental studies

Experimental investigation often targets the measurement of the static binding capacity q_{eq}, measured through the variation of the initial concentrations (C_0) and the equilibrium concentrations (C_e) of the adsorbate in the liquid, where the adsorbent is suspended. The amount of uremic toxin adsorbed at equilibrium (q_{eq}) is calculated as:

$$q_{eq} = \frac{(C_0 - C_e)V}{W} \tag{5.1}$$

where V refers to the volume of the solution, and W is the weight of the dry adsorbent.

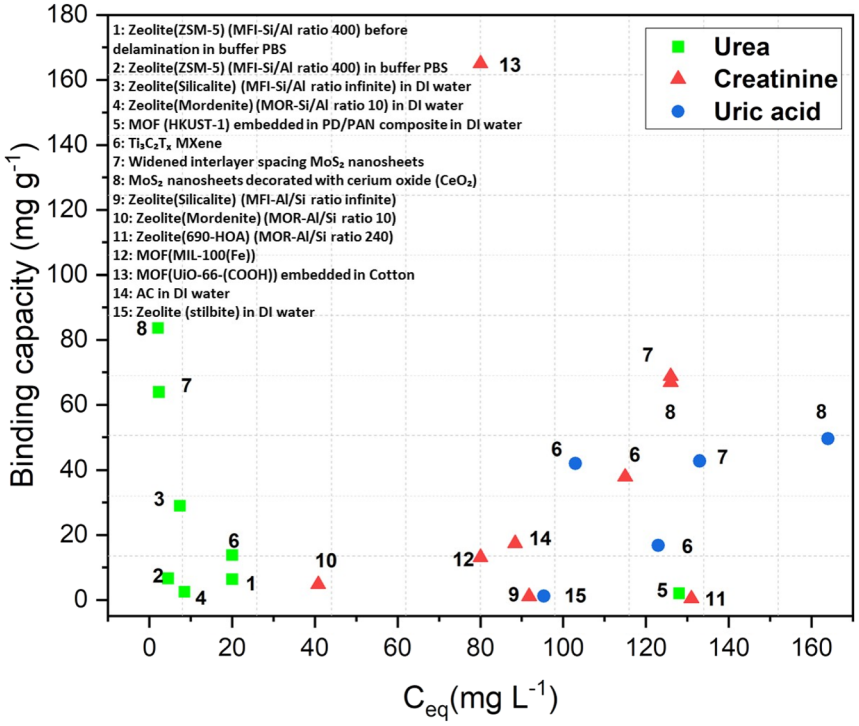

Figure 5.4: Experimentally measured UTs static binding capacity in several adsorbent materials. **Urea** for ZSM-5 before dealumination [42], ZSM-5 [43], silicalite [44], mordenite [44], HUKST-1 [24], Ti_3C_2Tx MXene [45], widened interlayer spacing MoS_2 nanosheets [46], (MoS_2) nanosheets decorated cerium oxide (CeO_2) ([47], p. 2), SBA-15 NH_2 [48], SBA-15 [48], **Creatinine** for silicalite [44], mordenite [44], 690-HOA [49], MIL-100(Fe) [50], UiO-66-$(COOH)_2$ [51], AC [41], Ti_3C_2Tx MXene [52], widened interlayer spacing MoS_2 nanosheets [46], (MoS_2) nanosheets decorated cerium oxide (CeO_2) ([47], p. 2), and **Uric acid** for stilbite [44], Ti_3C_2Tx MXene [52], widened interlayer spacing MoS_2 nanosheets [46], (MoS_2) nanosheets decorated cerium oxide (CeO_2) ([47], p. 2), at equilibrium concentration (Ceq), based on literature data.

Considering experimental studies, UTs binding capacities of the aforementioned nanoporous materials at equilibrium concentration for urea, creatinine, uric acid, and hippuric acid (HA) were investigated. Figure 5.4 summarizes the obtained q_{eq} at specific C_e for adsorption of urea, creatinine, and uric acid on various nanoporous materials.

Considering the experimental studies of urea adsorption, Fabiani et al. [53] calculated the static binding capacity of urea adsorption on nanoporous materials at C_{eq} = 5 mM, a typical concentration of urea expected in the spent dialysate. It was reported that the best performing adsorbents are nanomaterials of HKUST-1 embedded in polydopamine/polyacrylonitrile (PAN/PD) composite [24], MoS_2 with widened interlayer spacing [37], SBA-15 NH_2 [19], SBA-15 [19], silicalite (MFI) [10], AC [3], MXene (Ti_3C_2Tx) [33], ZSM-5 (Si/Al ratio 400) [6], mordenite (MOR) [10] showed the binding capacity of 320, 138.9, 50.5, 29.8, 19.6, 4.4, 3.5, 1.6, and 1.47 mg g^{-1}, respectively.

5.3.2.2 Computational modelling

In the study of UTs adsorption by nanoporous materials for dialysate regeneration, computational modelling plays a crucial role in exploring underlying mechanisms and optimizing material performances. In molecular simulations atoms are modelled as spheres interacting according to a force field, dictating their relative movements and interactions. The main methods used involve either MonteCarlo (MC), molecular dynamics (MD), or density functional theory (DFT) methodologies. The detailed discussion and introduction of these methodologies is out of the scope of the present review and we address the reader to other reviews [54, 55].

The adsorption of urea, creatinine, uric acid, indoxyl sulfate, and *p*-cresol on nanomaterials has been investigated by several authors using molecular modelling. Table 5.2 summarises the computational researches utilizing the MD, MC, and DFT calculations to study the UTs adsorption by nanomaterials. Jokar et al. [56] explored the adsorption of urea on various nanomaterials such as boron-carbon-nitride (BCN) nanolayers, BCN–nanotubes, graphene, carbon nanotubes (CNTs), and zeolite nanoparticles, finding that BCN nanomaterials exhibited the highest urea adsorption due to strong van der Waals (VDW) and electrostatic interactions with urea molecules, along with favorable Gibbs free energy. In a study by Wernert et al. [57], silicalite zeolites demonstrated significant adsorption potential for para-cresol, with 12 molecules adsorbed per unit cell, amounting to 112.8 mg g^{-1}. Palabıyık et al. [58] examined bio-compatible MOFs and identified OREZES, a carboxylate-based MOF, as highly selective for urea/water separation, while BEPPIX, an amino-based MOF, showed strong selectivity for creatinine/water separation with an exceptionally high separation factor. Yıldız et al. [59] further evaluated MOFs, identifying adenine-based bio-MOFs, specifically bio-MOF-11 (YUVSUE) and bio-MOF-12 (BEYSEF), and a dicyanamide-based MOF (KEXDIB) as promising for both urea and creatinine separations due to their molecular properties. Fabiani et al. [60] studied a broad range of 560 nanoporous materials, finding that the excess chemical potential for urea adsorption increased markedly with fluorine content, highlighting a potential design principle for improving urea adsorption in COFs. Li et al. [61] demonstrated that MOFs with aromatic ligands and carboxylic acid groups exhibit excellent adsorption capabilities for indoxyl sulfate, surpassing 2,100 mg g^{-1}. Investigating the adsorption of urea on doped graphene, Karimi et al. [62] found that nitrogen-doped graphene nanosheets (10 % nitrogen) achieved the best adsorption performance based on total and adsorption energy metrics. Meanwhile, Bergé-Lefranc et al. [63] observed a high adsorption rate of both urea and indoxyl sulfate in silicalite zeolite under maximum site occupancy, achieving 1.034 mmol g^{-1}. Jahromi et al. [64, 65] evaluated N- and P-doped fullerenes and specific COFs, revealing that N-doped fullerenes (8 % nitrogen) enhanced hydrogen bonding and adsorption energy for urea, while the TPA-COF modified with–OH functional groups exhibited improved urea adsorption. Skorane et al. [66] investigated azacalix [*n*]arenes (ACAs)-COFs for uric acid and creatinine adsorption, reporting consistent performance even in saline conditions, making it suitable for biofiltration applications. Lastly, Zandi et al. [67] explored MXene nanosheets and found that Cd_2C-based MXene exhibited the best stability

Table 5.2: Summary of the computational researches on UTs adsorption by nanomaterials.

	Method	UTs	Nanomaterial
Jokar et al. [56]	MD	Urea	Boron-carbon-nitride (BCN) nanolayer, BCN–nanotube, graphene, carbon nanotube (CNT), zeolite Y, zeolite Z, and zeolite ZSM5 nanoparticles having various surface areas.
Wernert et al. [57]	GCMC	*para*-Cresol	Silicalite zeolite
Palabıyık et al. [58]	GCMC MD	Urea, Creatinine	60 bio-compatible MOFs
Yıldız et al. [59]	GCMC	Urea, Creatinine	122 bio-MOFs
Fabiani et al. [60]	MC and MD	Urea	560 nanoporous material comprising COFs, some siliceous zeolites, MOFs and graphitic materials.
Li et al. [61]	GCMC	Indoxyl sulfate	Biocompatible MoFs
Karimi et al. [62]	MD	Urea	Nitrogen-doped and phosphorus-doped graphene
Bergé-lefranc [63] et al.	GCMC	Urea, Indoxyl Sulfate	Silicalite zeolite (MFI,Si/Al = 30)
Jahromi et al. [64]	MD	Urea	N- and P-doped fullerenes
Jahromi et al. [65]	MD DFT	Urea	TPA-COF, DAAQ-TFP, DAPHTFP, Tp-PaSO3Li–COF, PHOS–COF
Skorane et al. [66]	MD	Uric acid, creatinine	Azacalix [*n*]arenes (ACAs)-CoF
Zandi et al. [67]	MD	Urea	MXene nanosheets including Mn_2C, Cd_2C, Cu_2C, Ti_2C, W_2C, Ta_2C,

and adsorption properties for urea, demonstrating potential for further exploration in practical adsorption applications.

Machine Learning (ML) methods. The continuous expansion of databases for nanoporous materials, particularly COFs and MOFs, has introduced challenges in computational screening due to high computational costs and slower processing times. ML offers a solution by significantly reducing calculation time, thus enhancing the efficiency of large-scale screenings. Recent advancements in ML methods have accelerated the discovery and rational design of new materials by predicting the behaviour of adsorbate-nanoporous systems. By analysing large datasets of nanoporous materials descriptors and computational results, ML can uncover relationships between material composition, structure as features, and performance as target, ultimately helping identify the best-performing nanomaterials [68, 69]. Figure 5.5 represents a flowchart outlining the application of ML techniques to predict adsorption performance in nanomaterials. A typical ML-based study on adsorption processes begins with obtaining parameters defining the adsorption performance from simulations, which serve as targets for the ML model. Next, specific descriptors (features) related to nanomaterials, such

as structural and chemical properties, are selected to form the dataset. The dataset is then split into training and test sets, followed by applying a scaling technique to standardize the data. The model is trained on the training set, with hyperparameters optimized to improve performance. The accuracy of the model is evaluated using metrics like R^2 (coefficient of determination) and RMSE (root mean square error). The values of R^2 and RMSE can be calculated using the equations shown below [70].

$$R^2 = 1 - \frac{\sum_{i=1}^{n} \left(y_i - y_i^*\right)^2}{\sum_{i=1}^{n} \left(y_i - \bar{y}\right)^2}, \tag{5.2}$$

$$\text{RMSE} = \sqrt{\frac{\sum_{i=1}^{n} \left(y_i - y_i^*\right)^2}{n}}, \tag{5.3}$$

where $\bar{y}$ refers to the mean value of the actual responses, and y_i^*, y_i relate to predicted and actual values of the ith sample response, respectively. The value of n corresponds to the number of samples in the dataset.

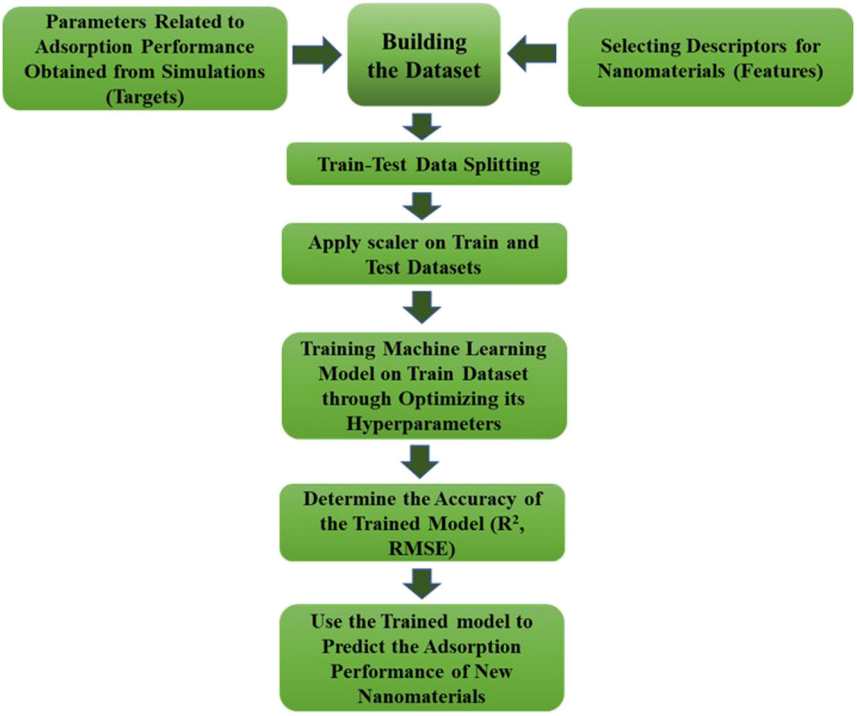

Figure 5.5: Flow chart representing the steps involved in training machine learning models.

Once the model is validated, it can be used to predict the adsorption performance of new nanomaterials, facilitating faster discovery of optimal adsorbents.

Despite the lack of specific studies applying ML to the adsorption of UTs from water solutions, there is a growing body of research on the use of ML in water treatment. For instance, Malloum et al. [54] reviewed the computational research and ML approaches targeting the adsorption process for water treatment. Lowe et al. [71] reviewed the application of ML in adsorption-based water treatment. ML models, such as random forest (RF), artificial neural networks (ANN), and support vector machines (SVM), have been extensively trained to predict the adsorption efficiency of pollutants onto adsorbents like attapulgite clay [72], nickel (II) oxide nanocomposites [73], activated carbon [74], and encapsulated nanoscale zero-valent iron [75], often achieving R^2 values greater than 0.9.

It is worth noting that, given the extensive data screening on the adsorption of UTs using large databases of MOFs and covalent organic COFs, ML can be effectively combined with simulation techniques to uncover correlations between material features (descriptors of porous materials) and target properties (such as the calculated binding capacity of adsorbents).

Our group developed for the first time a method to assess, using ML, the urea removal performance of a set of COFs based on a set of structural descriptors such as the largest included sphere (LIS), available surface area (ASA), and probe-occupiable volume accessible (POVA) along with chemical features like atomic composition percentages. The excess chemical potential of adsorption for urea and water molecules by COFs, estimated by Fabiani et al. from atomistic simulations, was used as target [53].

RF regressor is an "ensemble learning" method that combines a large number of decision trees, effectively reducing variance when compared to using individual decision trees [76]. RF algorithm constructs K regression trees and computes the average of their outputs. Once K trees $\{T(x)\}_1^K$ are generated, the RF regression predictor is expressed as [77]:

$$\widehat{f}_{RF}^{K}(x) = \frac{1}{k}\sum_{k=1}^{K} T(x) \tag{5.4}$$

The performance of the Random Forest model was assessed using R^2 scores on both training and testing datasets, indicating the model's capacity to capture the relationships between descriptors and target properties. Specifically, the training R^2 scores were 0.88 for excess chemical potential of urea and 0.92 for excess chemical potential of water, suggesting strong predictive performance on the training data. The testing R^2 scores, at 0.58 excess chemical potential of urea and 0.650 for excess chemical potential of water, indicate moderate generalizability on unseen data, with potential for further model refinement to enhance predictive accuracy on new samples. Figure 5.6 shows the predicted performance versus the one obtained via atomistic simulations.

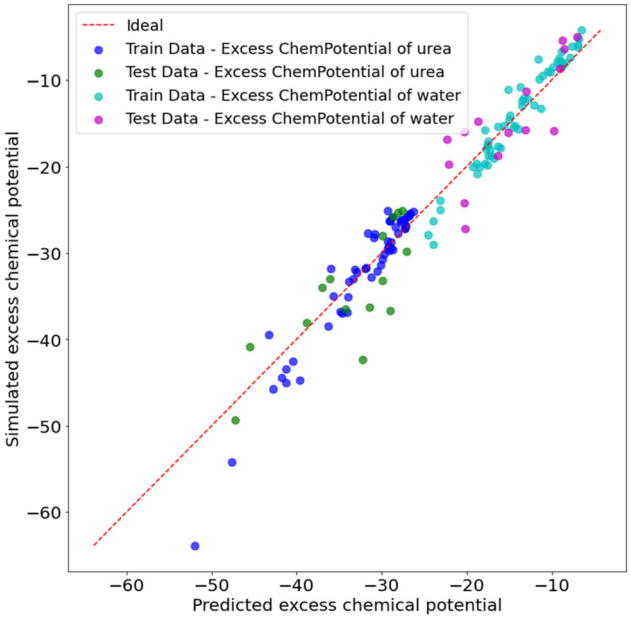

Figure 5.6: Simulated values of excess chemical potential versus predicted excess chemical potential obtained from RF model training (this work).

5.4 Conclusions

The creation of a wearable hemodialysis device could significantly boost patient outcomes and enhance their quality of life, while also easing pressures on healthcare facilities and decreasing water consumption. However, a key technical obstacle is the necessity for effective regeneration of spent dialysate, particularly achieving the complete removal of urea and other harmful toxins.

Historically, the management of urea in wearable dialysis prototypes has utilised chemical methods like oxidation and enzymatic conversion, key features in prototype models. These techniques, however, have considerable limitations due to the creation of toxic by-products such as ammonia and carbon dioxide. On the other hand, physical methods like adsorption and forward osmosis-enhanced HD offer a safer alternative but still do not achieve complete urea removal in a compact and efficient manner.

Recent advances in nanoporous materials and improved computational design tools have reignited interest and made strides in sorbent technologies for dialysate purification and in developing wearable kidney devices. Innovative experimental research has revealed various promising new porous materials for cleansing spent dialysate, though these initial findings require further verification through extended studies to confirm reproducibility and effectiveness under clinically relevant conditions. Concurrently,

advancements in computational techniques, including molecular simulations and machine learning, have greatly extended the scope of material testing beyond standard lab methods, accelerating the development and optimisation of materials for toxin elimination. Additionally, molecular techniques may enable the identification of sorbent materials capable of selectively capturing not just standard uremic toxins like urea and creatinine but also more harmful substances with less effort than traditional trial-and-error methods. These techniques facilitate the screening of material families such as covalent organic frameworks (COFs), known for their high tunability and water stability and the absence of potentially harmful metals.

Machine learning, when properly trained with experimental or simulated data, can screen broader arrays of nanoporous crystalline sorbents than atomistic simulations alone, extending performance predictions to novel, yet-to-be-synthesized materials. This opens avenues for efficient reverse material design and we have applied this method to the screening of a family of COFs for the removal of urea from water.

Chemical engineers, with their comprehensive skills in computational modelling, physics, chemistry, and process design, and their ability to collaborate across disciplines, are ideally suited to lead these innovations. Such technological advances are propelling us toward the realisation of wearable artificial kidneys – a significant leap forward that promises to markedly improve patient health and stands as a groundbreaking field in chemical engineering applied to medicine.

Acknowledgments: The authors would like to thank the editors David Bogle and Tomasz Sosnowski for their guidance and review of this article before its publication.

References

1. Kirwan C, Frankel A. The artificial kidney. In: Hakim NS, editor. Artificial Organs. London: Springer; 2009: 39–55 pp.
2. Chronic kidney disease – the lancet. [Online]. https://www.thelancet.com/article/S0140-6736(16)32064-5/abstract [Accessed 23 Jul 2024].
3. Finco DR. Chapter 17 – kidney function. In: Kaneko JJ, Harvey JW, Bruss ML, editors. Clinical Biochemistry of Domestic Animals, 5th ed. San Diego: Academic Press; 1997:441–84 pp.
4. Lisowska-Myjak B. Uremic toxins and their effects on multiple organ systems. Nephron Clin Pract 2014;128: 303–11.
5. Neirynck N, de Smet R, Schepers E, Vanholder R, Glorieux G. Classification and a list of uremic toxins. In: Uremic Toxins. Hoboken, NJ, USA: John Wiley & Sons, Inc; 2012:13–33 pp.
6. Eutox. The European uremic toxins (EUTox) database. [Online]. www.uremic-toxins.org [Accessed 09 Sep 2024].
7. Vanholder R, Pletinck A, Schepers E, Glorieux G. Biochemical and clinical impact of organic uremic retention solutes: a comprehensive update. Toxins (Basel) 2018;10:33.
8. Kalantar-Zadeh K, Jafar TH, Nitsch D, Neuen BL, Perkovic V. Chronic kidney disease. Lancet 2021;398: 786–802.

9. National kidney foundation practice guidelines for chronic kidney disease: evaluation, classification, and stratification. [Online]. https://www.acpjournals.org/doi/epdf/10.7326/0003-4819-139-2-200307150-00013.[Accessed 15 May 2024].
10. Couser WG, Remuzzi G, Mendis S, Tonelli M. The contribution of chronic kidney disease to the global burden of major noncommunicable diseases. Kidney Int 2011;80:1258–70.
11. Astley ME, Boenink R, Abd ElHafeez S, Trujillo-Alemán S, Arribas F, Åsberg A, et al. The ERA Registry annual report 2020: a summary. Clin Kidney J 2023;16:1330–54.
12. Bello AK, Johnson DW, Feehally J, Harris D, Jindal K, Lunney M, et al. Global kidney health atlas (GKHA): design and methods. Kidney Int Suppl 2017;7:145–53.
13. Ledebo I, Blankestijn PJ. Haemodiafiltration – optimal efficiency and safety. NDT Plus 2010;3:8–16.
14. Azar AT, Canaud B. Hemodialysis system. In: Azar AT, editor. Modelling and control of dialysis systems: volume 1: modeling techniques of hemodialysis systems. Berlin, Heidelberg: Springer; 2013:99–166 pp.
15. Ronco C and Clark WR. Haemodialysis membranes. Nat Rev Nephrol 2018;14. https://doi.org/10.1038/s41581-018-0002-x.
16. Mohajerani F, Clark WR, Ronco C, Narsimhan V. Mass transport in high-flux hemodialysis: application of engineering principles to clinical prescription. Clin J Am Soc Nephrol 2022;17:749.
17. Influence of dialysis membranes on clinical outcomes: from history to innovation. [Online]. https://www.mdpi.com/2077-0375/12/2/152.[Accessed 20 Dec 2024].
18. Azar AT, Canaud B. Hemodialysis system. In: Modelling and control of dialysis systems, in studies in computational intelligence. Berlin, Heidelberg: Springer Berlin Heidelberg; 2013:99–166 pp.1
19. Ahmad S. Manual of clinical dialysis, 2nd ed. 2009 edition US, New York: Springer; 2014.
20. van Gelder MK, Mihaila SM, Jansen J, Wester M, Verhaar MC, Joles JA, et al. From portable dialysis to a bioengineered kidney. Expet Rev Med Dev 2018;15:323–36.
21. Geremia I, Jong JAW, van Nostrum CF, Hennink WE, Gerritsen KGF, Stamatialis D. New mixed matrix membrane for the removal of urea from dialysate solution. Sep Purif Technol 2021;277:119408.
22. Jaffrin MY, Ding LH, Laurent JM. Simultaneous convective and diffusive mass transfers in a hemodialyser. J Biomech Eng 1990;112:212–19.
23. Daugirdas JT. Simplified equations for monitoring Kt/V, PCRn, eKt/V, and ePCRn. Adv Ren Replace Ther 1995;2:295–304.
24. Fiore GB, Guadagni G, Lupi A, Ricci Z, Ronco C. A new semiempirical mathematical model for prediction of internal filtration in hollow fiber hemodialyzers. Blood Purif 2006;24:555–68.
25. Oshvandi K, Kavyannejad R, Borzuo SR, Gholyaf M. High-flux and low-flux membranes: efficacy in hemodialysis. Nurs Midwifery Stud 2014;3:e21764.
26. Leypoldt JK, Cheung AK. Removal of high-molecular-weight solutes during high-efficiency and high-flux haemodialysis. Nephrol Dial Transplant 1996;11:329–35.
27. Vienken J. Membranes for haemodialysis. What is more important, sieving coefficient or flux? Probl Eksploat 2013:7–16.
28. Hulko M, Haug U, Gauss J, Boschetti-de-Fierro A, Beck W, Krause B. Requirements and pitfalls of dialyzer sieving coefficients comparisons. Artif Organs 2018;42:1164–73.
29. A wearable artificial kidney for patients with end-stage renal disease – PMC. [Online]. https://www.ncbi.nlm.nih.gov/pmc/articles/PMC4936831/.[Accessed 29 Jul 2024].
30. Chiu Y-W, Teitelbaum I, Misra M, de Leon EM, Adzize T, Mehrotra R. Pill burden, adherence, hyperphosphatemia, and quality of life in maintenance dialysis patients. Clin J Am Soc Nephrol 2009;4:1089.
31. Shao G, Himmelfarb J, Hinds BJ. Strategies for optimizing urea removal to enable portable kidney dialysis: a reappraisal. Artif Organs 2022;46:997–1011.
32. Gura V, Rivara MB, Bieber S, Munshi R, Smith NC, Linke L, et al. A wearable artificial kidney for patients with end-stage renal disease. JCI Insight 2016;1:e86397.

33. Dou P, Donato D, Guo H, Zhao S, He T. Recycling water from spent dialysate by osmotic dilution: impact of urea rejection of forward osmosis membrane on hemodialysis duration. Desalination 2020;496:114605.
34. Shaffer DL, Werber JR, Jaramillo H, Lin S, Elimelech M. Forward osmosis: where are we now? Desalination 2015;356:271–84.
35. Vollenbroek JC, Rodriguez AP, Mei BT, Mul G, Verhaar MC, Odijk M, et al. Light-driven urea oxidation for a wearable artificial kidney. Catal Today 2023:114163. https://doi.org/10.1016/j.cattod.2023.114163.
36. Shao G, et al. Dialysate regeneration via urea photodecomposition with TiO2 nanowires at therapeutic rates. Artif Organs 2023. https://doi.org/10.1111/aor.14514.
37. Wu D, Xu F, Sun B, Fu R, He H, Matyjaszewski K. Design and preparation of porous polymers. Chem Rev 2012;112:3959–4015.
38. Grassi M, Kaykioglu G, Belgiorno V, Lofrano G. Removal of emerging contaminants from water and wastewater by adsorption process. In: Lofrano G, editor. Emerging Compounds Removal from Wastewater: Natural and Solar Based Treatments. Dordrecht: Springer Netherlands; 2012:15–37 pp. in SpringerBriefs in Molecular Science.
39. Ma Y, Li S, Tonelli M, Unsworth LD. Adsorption-based strategies for removing uremic toxins from blood. Microporous Mesoporous Mater 2021;319:111035.
40. van Gelder MK, Jong JA, Folkertsma L, Guo Y, Blüchel C, Verhaar MC, et al. Urea removal strategies for dialysate regeneration in a wearable artificial kidney. Biomaterials 2020;234:119735.
41. Kameda T, Horikoshi K, Kumagai S, Saito Y, Yoshioka T. Adsorption of urea, creatinine, and uric acid onto spherical activated carbon. Separ Purif Technol 2020;237:116367.
42. De Pascale M, De Angelis MG, Boi C. Mixed matrix membranes adsorbers (MMMAs) for the removal of uremic toxins from dialysate. Membranes 2022;12. https://doi.org/10.3390/membranes12020203.
43. Cheng Y-C, Fu C-C, Hsiao Y-S, Chien C-C, Juang R-S. Clearance of low molecular-weight uremic toxins p-cresol, creatinine, and urea from simulated serum by adsorption. J Mol Liq 2018;252:203–10.
44. Wernert V, Schäf O, Ghobarkar H, Denoyel R. Adsorption properties of zeolites for artificial kidney applications. Microporous Mesoporous Mater 2005;83:101–13.
45. Meng F, Seredych M, Chen C, Gura V, Mikhalovsky S, Sandeman S, et al. MXene sorbents for removal of urea from dialysate: a step toward the wearable artificial kidney. ACS Nano 2018;12:10518–28.
46. Zhao H, Huang J, Miao L, Yang Y, Xiao Z, Chen Q, et al. Toward urease-free wearable artificial kidney: widened interlayer spacing MoS2 nanosheets with highly effective adsorption for uremic toxins. Chem Eng J 2022;438:135583.
47. Zhao H, Huang J, Huang L, Yang Y, Xiao Z, Chen Q, et al. Surface control approach for growth of cerium oxide on flower-like molybdenum disulfide nanosheets enables superior removal of uremic toxins. J Colloid Interface Sci 2023;630:855–65.
48. Nguyen CH, Fu C-C, Chen Z-H, Tran TTV, Liu S-H, Juang R-S. Enhanced and selective adsorption of urea and creatinine on amine-functionalized mesoporous silica SBA-15 via hydrogen bonding. Microporous Mesoporous Mater 2021;311:110733.
49. Sasaki M, Liu Y, Ebara M. Zeolite composite nanofiber mesh for indoxyl sulfate adsorption toward wearable blood purification devices. Fibers 2021;9. https://doi.org/10.3390/fib9060037.
50. Yang C-X, Liu C, Cao Y-M, Yan X-P. Metal–organic framework MIL-100(Fe) for artificial kidney application. RSC Adv 2014;4:40824–7.
51. Abdelhameed RM, Rehan M, Emam HE. Figuration of Zr-based MOF@cotton fabric composite for potential kidney application. Carbohydr Polym 2018;195:460–7.
52. Zhao Q, Seredych M, Precetti E, Shuck CE, Harhay M, Pang R, et al. Adsorption of uremic toxins using Ti3C2Tx MXene for dialysate regeneration. ACS Nano 2020;14:11787–98.
53. Fabiani T, Zarghamidehaghani M, Boi C, Dimartino S, Kentish S, De Angelis MG. Sorbent-based dialysate regeneration for the wearable artificial kidney: advancing material innovation via experimental and computational studies. Separ Purif Technol 2025;360:130776.

54. Malloum A, Adegoke KA, Ighalo JO, Conradie J, Ohoro CR, Amaku JF, et al. Computational methods for adsorption study in wastewater treatment. J Mol Liq 2023;390:123008.
55. Chen J. The development and comparison of molecular dynamics simulation and Monte Carlo simulation. IOP Conf Ser Earth Environ Sci 2018;128:012110.
56. Jokar Z, Khademiyan A, Fallah M-A, Smida K, Sajadi SM, Inc M. Molecular dynamics simulation of urea adsorption on various nanoparticles in a spiral microfluidic system. Eng Anal Bound Elem 2022;145:271–85.
57. Wernert V, Schäf O, Faure V, Brunet P, Dou L, Berland Y, et al. Adsorption of the uremic toxin p-cresol onto hemodialysis membranes and microporous adsorbent zeolite silicalite. J Biotechnol 2006;123:164–73.
58. Akkoca Palabıyık B, Batyrow M, Erucar I. Computational investigations of Bio-MOF membranes for uremic toxin separation. Separ Purif Technol 2022;281:119852.
59. Yıldız T, Erucar I. Revealing the performance of bio-MOFs for adsorption-based uremic toxin separation using molecular simulations. Chem Eng J 2022;431:134263.
60. Fabiani T, Ricci E, Boi C, Dimartino S, Angelis MGD. In silico screening of nanoporous materials for urea removal in hemodialysis applications. Phys Chem Chem Phys 2023;25:24069–80.
61. Li B, Gong S, Cao P, Gao W, Zheng W, Sun W, et al. Screening of biocompatible MOFs for the clearance of indoxyl sulfate using GCMC simulations. Ind Eng Chem Res 2022;61:6618–27.
62. Karimi K, Rahsepar M. Optimization of the urea removal in a wearable dialysis device using nitrogen-doped and phosphorus-doped graphene. ACS Omega 2022;7:4083–94.
63. Bergé-Lefranc D, Pizzala H, Paillaud JL, Schäf O, Vagner C, Boulet P, et al. Adsorption of small uremic toxin molecules on MFI type zeolites from aqueous solution. Adsorption 2008;14:377–87.
64. Miri Jahromi A, Zandi P, Khedri M, Ghasemy E, Maleki R, Tayebi L. Molecular insight into optimizing the N- and P-doped fullerenes for urea removal in wearable artificial kidneys. J Mater Sci Mater Med 2021;32:49.
65. Jahromi AM, Khedri M, Ghasemi M, Omrani S, Maleki R, and Rezaei N. Molecular insight into COF monolayers for urea sorption in artificial kidneys. Sci Rep 2021;11. https://doi.org/10.1038/s41598-021-91617-1.
66. Skorjanc T, Shetty D, Gándara F, Pascal S, Naleem N, Abubakar S, et al. Covalent organic framework based on azacalix[4]arene for the efficient capture of dialysis waste products. ACS Appl Mater Interfaces 2022;14:39293–8.
67. Zandi P, Ghasemy E, Khedri M, Rashidi A, Maleki R, Miri Jahromi A. Shedding light on miniaturized dialysis using MXene 2D materials: a computational chemistry approach. ACS Omega 2021;6:6312–25.
68. Yan Y, Zhang L, Li S, Liang H, Qiao Z. Adsorption behavior of metal-organic frameworks: from single simulation, high-throughput computational screening to machine learning. Comput Mater Sci 2021;193:110383.
69. Nagasubramanian S. The future of the artificial kidney. Indian J Urol 2021;37:310.
70. Hamed Mashhadzadeh A, Zarghami Dehaghani M, Kadyr A, Golman B, Spitas C, et al. Machine Learning-Assisted design of boron and nitrogen doped graphene nanosheets with tailored thermomechanical properties. Comput Mater Sci 2024;240:112998.
71. Lowe M, Qin R, Mao X. A review on machine learning, artificial intelligence, and smart technology in water treatment and monitoring. Water 2022;14. https://doi.org/10.3390/w14091384.
72. Bhagat SK, Pyrgaki K, Salih SQ, Tiyasha T, Beyaztas U, Shahid S, et al. Prediction of copper ions adsorption by attapulgite adsorbent using tuned-artificial intelligence model. Chemosphere 2021;276:130162.
73. Mazloom MS, Rezaei F, Hemmati-Sarapardeh A, Husein MM, Zendehboudi S, Bemani A. Artificial intelligence based methods for asphaltenes adsorption by nanocomposites: application of group method of data handling, least squares support vector machine, and artificial neural networks. Nanomaterials 2020;10. https://doi.org/10.3390/nano10050890.
74. Mesellem Y, Hadj AAE, Laidi M, Hanini S, Hentabli M. Computational intelligence techniques for modeling of dynamic adsorption of organic pollutants on activated carbon. Neural Comput Applic 2021;33:12493–512.
75. Mahmoud AS, Mostafa MK, Nasr M. Regression model, artificial intelligence, and cost estimation for phosphate adsorption using encapsulated nanoscale zero-valent iron. Separ Sci Technol 2019;54:13–26.

76. Couronné R, Probst P, Boulesteix A-L. Random forest versus logistic regression: a large-scale benchmark experiment. BMC Bioinf 2018;19:270.
77. Machine learning predictive models for mineral prospectivity: an evaluation of neural networks, random forest, regression trees and support vector machines – ScienceDirect. [Online]. https://www.sciencedirect.com/science/article/pii/S0169136815000037.[Accessed 20 Dec 2024].